NANO LETTERS

2006
Vol. 6, No. 9
1993−1999

Quantum Dot Encapsulation in Viral Capsids

Suraj K. Dixit,[†] Nancy L. Goicochea,[†] Marie-Christine Daniel,[†] Ayaluru Murali,[||] Lyudmila Bronstein,[†] Mrinmoy De,[‡] Barry Stein,[§] Vincent M. Rotello,[‡] C. Cheng Kao,[||] and Bogdan Dragnea*,[†]

Department of Chemistry, Indiana University, Bloomington, Indiana 47405, Department of Chemistry, University of Massachusetts-Amherst, Amherst, Massachusetts 01002, Indiana Molecular Biology Institute, Indiana University, Bloomington, Indiana 47405, and Department of Biochemistry & Biophysics, Texas A&M University, College Station, Texas 77843

Received May 22, 2006; Revised Manuscript Received July 8, 2006

ABSTRACT

Incorporation of CdSe/ZnS semiconductor quantum dots (QDs) into viral particles provides a new paradigm for the design of intracellular microscopic probes and vectors. Several strategies for the incorporation of QDs into viral capsids were explored; those functionalized with poly(ethylene glycol) (PEG) can be self-assembled into viral particles with minimal release of photoreaction products and enhanced stability against prolonged irradiation.

Introduction. Nanoparticle−biomaterial conjugates have a variety of highly useful properties that can be utilized for biosensing applications.[1−4] One application is the continuous tracking of viral infection,[5,6] which could lead to knowledge useful to prevent the initial steps of viral infection. The remarkable photostability and brightness of quantum dots (QD)[1] will allow long-term tracking of single virus particles. One strategy is to covalently modify the outside of virus particles with QD.[7,8] However, unless the position for the attachment of the QD on the capsid protein is selected carefully, the normal properties of viral infection will be affected. An alternative approach is to place the optical beacon inside the capsid, by partial or total replacement of the viral nucleic acid.[9]

Dragnea et al. used a self-assembly protocol to incorporate anionic gold nanoparticles with diameters ranging between 3 and 12 nm inside the capsids of a simple icosahedral virus, brome mosaic virus (BMV).[9−11] The nanoparticle−capsid complex assembly process is driven primarily by electrostatic interactions between the negatively charged gold nanoparticles and the positively charged internal compartment of the BMV capsid. The same principles of gold-core-templated self-assembly have been shown to be extensible to other icosahedral viruses.[12] PEG-coated gold-incorporated virus-like particles[11] (VLPs) are characterized by high efficiency of encapsidation and have been shown to possess symmetry and exhibit the physiochemical characteristics of viruses from the family *Bromoviridae*.[13] We demonstrate here how the requirements for the incorporation of QDs compare with those for incorporation of gold nanoparticles. From an applied point of view, if the same conditions exist for different cores, then it should be feasible to encapsidate other cores with desired properties as long as basic surface chemistry specifications are met. This analysis would also confirm the hypothesis that, similar to other self-organized mesoscopic systems, such as micelles,[14] the general principles underlying the virus self-assembly process can be used to control its outcome.

The strong luminescence of VLPs with encapsidated QDs holds promise as luminescent bioprobes. Nonetheless, there are a number of challenges in working with QDs for the formation of VLPs. First, upon light exposure, QDs could photorelease chemical species that would affect nearby macromolecules. For example, photoreleased Cd^{2+} ions could attack accessible cysteines in the capsid.[15] Second, the QDs need to be soluble in aqueous solutions. Although several methods have been worked out to achieve solubility, the close proximity between the QD and the capsid proteins may have additional specific requirements. Third, in working with the assembly of bromoviral capsids, one needs to keep pH values between approximately 5.0 and 7.5 because this range is required to stabilize the viral particles and induce capsid assembly.[16]

* Corresponding author. E-mail: dragnea@indiana.edu.
[†] Department of Chemistry, Indiana University.
[‡] University of Massachusetts-Amherst.
[§] Indiana Molecular Biology Institute, Indiana University.
[||] Texas A&M University.

10.1021/nl061165u CCC: $33.50
Published on Web 07/27/2006

In this study, several coatings for QDs were examined in an attempt to meet the above requirements, including lipid-micelles, streptavidin-biotin-DNA, DHLA (dihydrolipoic acid), and HS-poly(ethylene glycol) (PEG)-COOH. However, HS-PEG-COOH-coated QDs were the only systems found to yield stable and uniform QD/VLPs. We discuss here the assembly of QD-based VLPs, along with the photochemical properties of this system.

Experimental Section. *I. Synthesis of Functionalized Quantum Dots.* CdSe/ZnS nanocrystals were synthesized by using the lyothermal method reported previously.[17] Phospholipid micelle encapsulation of QDs was carried out using the method outlined by Dubertret et al.[18] TOPO (tri-octyl phosphine oxide)-coated QDs (2 mg) were suspended with 5.5 μmol of PEG-PE (1,2-diacyl-*sn*-glycero-3-phosphoethanolamine-*N*-[methoxy-poly(ethylene glycol)]) in chloroform followed by evaporation of the solvent and solubilization with water. Streptavidin-biotin-DNA-coated QDs were made by attaching commercially available streptavidin-coated QDs (Q-Dot Corporation, Hayward CA) to ssDNA that was chemically synthesized to contain a 5′ dual biotin (5′Bio/GTCTTCCGCTCTCGGCAGAGGTGTGAAGGA-3′).[19] This oligonucleotide contains the base sequence of the RNA motif required for BMV assembly in cells.[20] Streptavidin-coated QD conjugates emitting at 605 nm (6 μL, 1 μM) were mixed for 30 min at room temperature with an aqueous solution of biotinylated DNA (6 μL, 13 μM) and the incubation buffer (6 μL, pH = 8.4). The molar ratio of streptavidin-coated QDs to biotin-DNA is kept at 1:5 to ensure that every streptavidin on the QD is bound to at least one biotin-DNA. For simplicity, these particles will henceforth be named "DNA-coated QDs".

DHLA-coated QDs were obtained by exchange of TOPO from the CdSe/ZnS nanocrystals[21] with DHLA, using a similar strategy to synthesize HS-PEG-COOH-coated QDs.[22] Briefly, 1 mg of TOPO/TOP coated QDs suspended in 1 mL of chloroform were mixed with 10 mg of HS-PEG-COOH overnight at ~60−70 °C. The solvent was removed in a vacuum oven. The residue was then suspended in 1 mL of water (18 MΩ). The last step is accompanied by a change of the red residue to an orange, optically clear, transparent solution.

II. Characterization Methods. Dynamic light scattering (DLS, Zetasizer Nano-S, Malvern) of functionalized QDs in aqueous solution was performed to determine the hydrodynamic radii of the different functionalized dots. To prepare DLS samples, the master solution was diluted 10 times and sonicated for 1 h to prevent aggregation. The solution was subsequently filtered using a 0.1 μm syringe filter. The optical properties of the functionalized dots were characterized by fluorescence and absorption spectroscopy (Perkin-Elmer LS50B). The excitation wavelength used was 470 nm while the emission was scanned between 500 and 700 nm.

Gel electrophoresis was used to provide evidence for the anionic functional group attachment to the QD surface. The electrophoretic matrix was made of agarose gel (2%) in a TBE buffer [Tris base (0.4 M), boric acid (0.45 M), EDTA (10 mM)]. The sample was run at 7.5 V/cm, and the mobility of the sample was determined by measuring the relative displacements with a CCD-equipped stereo microscope.

Negative-stain transmission electronmicrographs of BMV-encapsulated QDs were taken by spreading a solution containing the viral capsid on a carbon-coated copper grid. Solution excess was removed with filter paper after 10 min, followed by addition of 10 μL of saturated uranyl acetate solution. After other 10 min, the stain excess on the grid was removed with filter paper. The sample was visualized with a transmission electron microscope (JEOL 1010) at 80 kV equipped with a digital camera.

III. Photostability Measurements of Functionalized QD Cores. Prior to measuring steady-state luminescence decays of functionalized QD samples as a function of the molecular coat, the samples were diluted and sonicated for ~1.5 h to avoid the presence of loosely bound aggregates. The samples were then exposed for 25 min to a 400 nm wavelength, doubled-frequency, amplified Ti-sapphire laser (RegA Model 9000, Coherent: average power, 90 mW; repetition rate, 250 kHz; pulse length, 200 fs). The 400 nm beam was split into two paths, one of which served as the reference, and the other one as the probe beam, which passed through a 1 mm path length three-way quartz cuvette. The laser beam filled the entrance window of the cuvette completely. The reference beam and the sample luminescence were detected by two pin Si photodiodes. Both reference and sample channels were gated using a box car integrator (Stanford Research, SRS 250). The luminescence intensity is then stored as a function of irradiation time. A digital thermocouple power meter was used to monitor the changes in the sample absorbance with respect to time.

IV. Assembly of VLPs Containing Functionalized QDs. The capsid subunits were obtained from BMV particles purified from infected plants as described in Dragnea et al.[9] To separate the capsid subunits from the BMV RNAs, 100 μL of intact BMV (~2 mg/mL) were dialyzed against a solution containing 0.5 M $CaCl_2$ solution at 4 °C for 24 h.[16] The insoluble material containing viral RNA was removed by centrifugation at 16 000 g for 20 min at 4 °C. The supernatant containing the dissociated proteins was then dialyzed against 0.01 M Tris base, pH 7.4 for 24 h at 4 °C to remove residual calcium ions and then dialyzed against TKM buffer (0.01 M Tris base + 1 M KCl + 0.005 M $MgCl_2$, pH 7.4) for 24 h at 4 °C.[16] The integrity of the capsid subunits was confirmed by MALDI-TOF (matrix-assisted laser desorption/ionization time-of-flight) mass spectrometry. Protein concentration was determined by UV−vis spectrometry. Capsid proteins prepared in this manner exist predominantly as stable dimers and can be used directly for VLP assembly.

To assemble the VLPs with QDs, one equivalent of functionalized QD's was usually mixed with 180 equivalents of capsid monomers (corresponding to a $T = 3$ VLP) and first dialyzed at 4 °C for 20 h against 100 mL of reassembly buffer (50 mM Tris base + 50 mM NaCl + 10 mM KCl + 5 mM $MgCl_2$, pH 7.4) the dialyzed against 100 mL of SAMA buffer (50 mM NaOAc + 8 mM $Mg(OAc)_2$, pH 4.5). The sample was kept at 4 °C. For HS-PEG-COOH-coated QDs, reassembly at other capsid subunit/core ratios was also

examined. The assembly reactions were placed in a centrifuge tube and underlayed with 400 μL of 10% sucrose solution in SAMA buffer to concentrate the VLPs and remove unassembled materials. Following centrifugation at 50 000 g for 0.5 h at 4 °C, the pellet containing the VLPs were resuspended in 100 μL of SAMA buffer.

IV. 3D TEM Reconstructions. Native BMV particles were purified from infected *Nicotiana benthamiana* leaves according to the protocol of Rao et al.[23] The purified virus was then sedimented through a 38.5% cesium chloride density column using a Beckman Ti60.1 rotor operated at 45 000 rpm for 36 h to separate the particles containing viral RNA and those that do not. The different preparations were collected and dialyzed in buffer V (0.1 M NaOAc, 1 mM EDTA, 10 mM $MgCl_2$, pH 5.0). The concentration of the virus was determined by its staining with Coomassie Blue against bovine serum albumin of known concentrations. The virus is stored in VB at −80 °C until use and diluted with VB, where appropriate.

Electron micrographs for quantum dots encapsulated with BMV coat proteins (QD-BMVs) and BMV particles purified from plants were taken on a JEOL 1200 EX transmission electron microscope operated at an accelerating voltage of 100 kV. Typically ca. 2 μL of sample (at 0.1 mg/mL) was spread on a glow-discharged carbon-coated copper grid, negatively stained and used for taking the electron micrographs. Electron micrographs were taken at a calibrated magnification of 38 900x at the specimen level and digitized using an Epson Projection 3200 scanner at 1200 dpi.

The 3D reconstructions were carried out using the EMAN software.[24] Typically about 2000 particles were taken for reconstructions. The particles were selected using EMAN's *boxer* program. The particles were filtered for high-frequency noise, centered, and aligned using EMAN's *cenalignint* program without applying any symmetry. An initial model was generated with EMAN's *starticos* program and was used for final reconstruction. The final reconstructions were visualized by UCSF's Chimera software.[25]

Results and Discussion. *I. Core Photostability.* As discussed above, photostabilty is crucial for QD encapsidation. The luminescence spectrum of the bare TOP/TOPO capped QDs exhibits a sharp peak at 574 nm, which corresponds to a diameter of 4 ± 0.6 nm.[17] This average size has been confirmed by TEM.

After functionalization, the hydrodynamic radius of various functionalized QDs in aqueous solution was characterized by DLS (Figure 1). The DLS size distributions are identical to the instrumental response function corresponding to a monodisperse sample, indicating that aggregation is negligible in all cases. A compilation of the number distribution measurements of the various functionalized QDs is given in Table 1.

Note that the hydrodynamic values are expected to be generally larger than the actual diameters because of counterion cloud contributions to particle mobility.[27]

To assess the photostability of different coatings, luminescence intensity and optical density of aqueous solutions of functionalized QDs have been recorded simultaneously

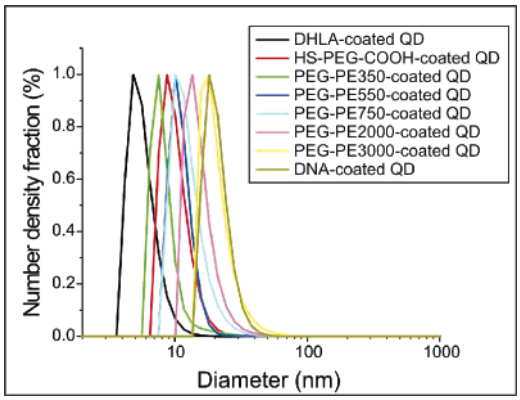

Figure 1. Dynamic light scattering distributions of functionalized QDs in aqueous solution.

Table 1. Diameters of Functionalized QD Diameters[22,26] as Measured by DLS[a]

ligand	DLS diam (nm)	expected diam (nm)
DHLA	6.5 ± 0.5	5
HS-PEG-COOH	8.5 ± 0.5	7
PEG-PE350	10 ± 0.5	11
PEG-PE550	13 ± 0.5	12
PEG-PE750	13.5 ± 0.5	14
PEG-PE2000	18.5 ± 1	17
PEG-PE3000	24 ± 1	23

[a] The expected diameters of functionalized QD assume fully extended chains and one monolayer coverage.

as a function of time and compared to bare CdSe/ZnS nanoparticles in chloroform (Figure 2a). A rapid initial increase in fluorescence occurs for all of the samples. The initial increase has been attributed to photoannealing, that is, a photoinduced reduction in the number of surface trap states, which results in an increase in the rate of radiant recombination.[28−30] A subsequent decrease in the fluorescence has been observed previously and is expected as a consequence of surface photooxidation facilitated by the presence of adsorbed water molecules.[29] In this case, the decrease in luminescence is usually accompanied by a small blue-shift of the excitation emission peak, indicative of surface oxidation.[29]

QDs coated with lipid-micelle, DNA, and DHLA all showed decreases in luminescence over the course of 800 s. However, concomitant with the decrease in luminescence, we also observe a ∼20% reduction in the optical density of the sample, suggesting that the luminescence decrease is due, at least in part, to removal of absorbers from the laser path, probably through aggregation and precipitation. Such aggregation may occur in response of a laser-induced, partial disruption of the water-soluble coating. The effects of the lengths of micelle used to coat the QD on the mobility of the reactive species (water, oxygen) was also examined.[29] A similar decay rate was observed for all of the QDs coated with PEG-PE of varying PEG lengths (Figure 2b). In addition, the decay rate to the PEG-PE coated QDs was similar to that of the DNA-coated QDs, perhaps due to these molecular coatings being stabilized by hydrophobic interactions.

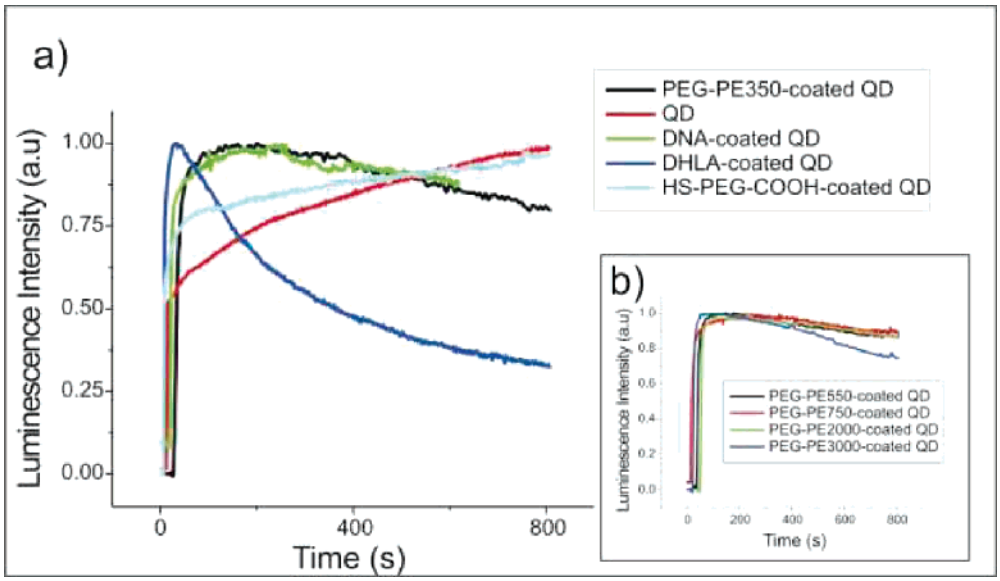

Figure 2. (a) Luminescence intensity as a function of irradiation time for different molecular coatings used to solubilize the QDs in water. (QD = bare QDs in chloroform). (b) QDs coated with PEG-PE of varying lengths.

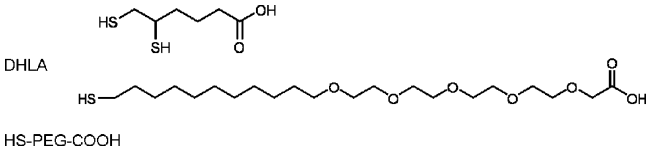

Figure 3. Molecular formulas of DHLA and HS-PEG-COOH.

Because the micelle coating should form a nonpolar barrier to decrease the rate of migration of reactive ionic species, we propose that the photodegradation involves species already adsorbed on the semiconductor surface. Note that HS-PEG-COOH-coated QDs have no significant luminescence decay over the course of the experiment, their behavior being similar to the bare QDs in chloroform (Figure 2a).

Although SH-PEG-COOH are anchored to the QD surface with the same covalent group as DHLA, the rate of decay for DHLA coated QDs is ~8 times faster. Increased stability of the HS-PEG-COOH-coated QDs is likely due to the structure of the PEG;[22] indeed, the C-11 carbon chain of HS-PEG-COOH can stack in a compact layer that could be responsible for a more robust coating. In contrast, the branched and less flexible structure of the DHLA[21] may not stack around the QD to the same degree (Figure 3).

II. VLP Assembly. A variety of viral capsids are known to readily assemble in vitro from homologous protein solutions upon a change in the buffer environment.[31,32] The mechanistic basis for the foreign core encapsulation in these conditions is probably due to tight association between subunits of the capsid and a high degree of nonspecific ionic interaction between the positively charged capsid subunits and the nucleic acid core.[33,34] In support of nonspecific interaction being at least a part of the requirement for assembly in vivo, VLPs can form in vivo and will encapsidate nonspecific cellular RNAs when the viral RNA is absent or limiting.[35,36]

BMV is a model small icosahedral virus with native capsids composed of 180 identical proteins of 20 kDa, which form a combination of pentameric and hexameric subunits.[13] A high-resolution structure of BMV is known from X-ray diffraction on intact virus crystals.[13] The BMV capsid is most stable at low to moderate ionic strength buffers with pH below 5.0, but experiences a profound structural transition when the pH is increased from 5 to 7. In the presence of Mg^{2+}, which stabilize the interaction of the capsid subunits, reversible expansion occurs without dissociation at neutral pH. At pH above 7.5 and ionic strength higher than 0.5 M, the capsid dissociates and the viral RNA precipitates. Upon reestablishment of low pH and ionic strength, reassociation occurs. These properties make BMV an ideal system to introduce functionalized nanoparticles inside the capsid.

Assembly of BMV capsids with the four types of functionalized QDs was attempted under the standard conditions detailed in the methods. Efficient incorporations (~75%) were observed with SH-PEG-COOH-coated QDs and DNA-coated QDs, but not with any of the lipid-micelle-coated or the DHLA-coated QDs. For the lipid-micelle-coated QDs, amorphous aggregation of protein−QD complexes was observed. Because interaction of the nonpolar protein domain with the lipids may occur due to the micelle fluid structure, protein denaturation by the micelle may be the cause of capsid formation failure. Capsid formation was also not observed with DHLA-coated QDs. In this case, the weak interaction of DHLA ligand with the QD surface could be responsible for ligand disruption in the presence of viral proteins. This assumption corroborates the photostability results.

The DNA-coated QDs yield VLPs that tend to be unstable in storage, as determined by DLS and TEM. Interestingly, the decay is accelerated by exposure to visible light (Figure 4a). We have studied this phenomenon for the PEG-COOH cores. Despite the fact that the SH-PEG-COOH-coated QDs cores are stable to laser exposure (Figure 2), VLPs containing the same cores tend to precipitate from solution (Figure 4b). Therefore, photochemistry products from the laser exposed

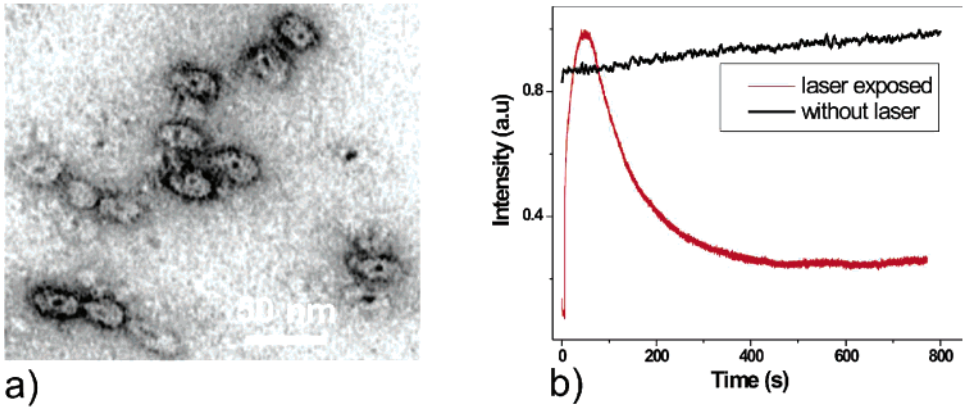

Figure 4. (a) TEM images of VLPs containing DNA-coated QDs (black dots). Note the elongated shape indicative of probable capsid structural damage. (b) The fluorescence from a QD-PEG-COOH VLP sample decays due to precipitation when the sample is exposed to a strong laser beam at 400 nm.

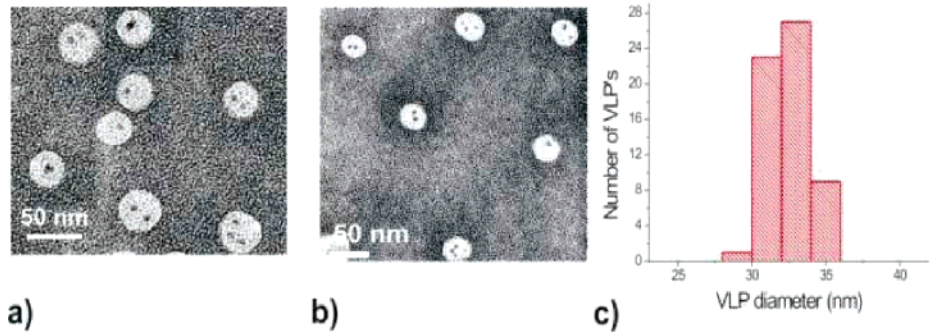

Figure 5. TEM images of VLPs containing HS-PEG-COOH-coated QDs. The equivalent ratios of QD to CP are 2:1 (a) and 3:1 (b), respectively. (c) Size histogram of VLPs corresponding to b.

core are probably affecting the integrity of protein shell only, which, in turn, results in aggregation. The PEG-COOH coating is not affected as the results in Figure 2 show. More investigations are necessary to elucidate the basis of this phenomenon.

At a ratio of 1:180 PEG-coated core to BMV capsid subunits, PEG-coated QDs produced regularly shaped particles expected for BMV (Figure 5a). VLP assembly was optimal when the stoichiometry of the PEG-coated core was at 2 or 3 equivalents of the capsid (Figure 5a and b). At 3 equivalents of PEG-coated QDs, ~75% of the VLPs contained PEG-coated cores, as determined by TEM imaging of the unpurified assembly reactions. Interestingly, the majority of the VLPs contained 2 or 3 QDs while their external diameter was 32 ± 1.4 nm as found from TEM data (Figure 5b,c).

TEM image reconstructions of single VLPs indicate that the protein shell structure corresponds to a $T = 2$ capsid, Figure 6a. The QD cores cannot be identified because they seem to reside at variable positions in the VLP and they will be averaged out in the reconstruction. The $T = 2$ capsid structure is shared by a form of BMV found in nature. The $T = 2$ μ_BV capsid has been isolated from a plant extract passed through a CsCl gradient that lacks RNAs. A reconstructed image of the $T = 2$ μ_BV is provided in Figure 6b. RNA-controlled 120-unit BMV capsid assembly has been also reported previously.[37]

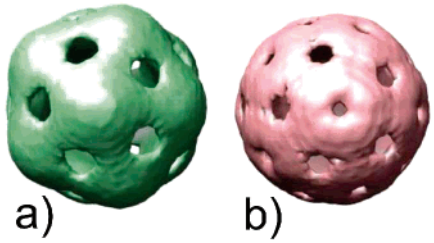

Figure 6. Image reconstruction of QD/BMV (a) and $T = 2$ BMV capsids isolated from plant extracts (b).

Similar to the gold particle incorporation, as the equivalents of HS-PEG-COOH-coated QDs increased from 1 to 4, the number of empty capsids decreased (Figure 7a). The optimum Au core size for a 28 nm BMV VLP has been found to be 12 nm,[10] with the percentage of core-containing VLPs being over 95%. The PEG-coated QDs are smaller than this optimum core size, having an initial diameter of 8.5 nm (Table 1).

A maximum ~75% yield of incorporation was obtained only when the QD cores were initially present at 2 and 3 equivalents of the capsid protein. In this case, the majority of the VLPs contained multiple cores. These results strongly suggest that a successful "nucleator" for capsid assembly requires a minimal core diameter and that the association between dimer or trimer of QDs improved the assembly of BMV particles.

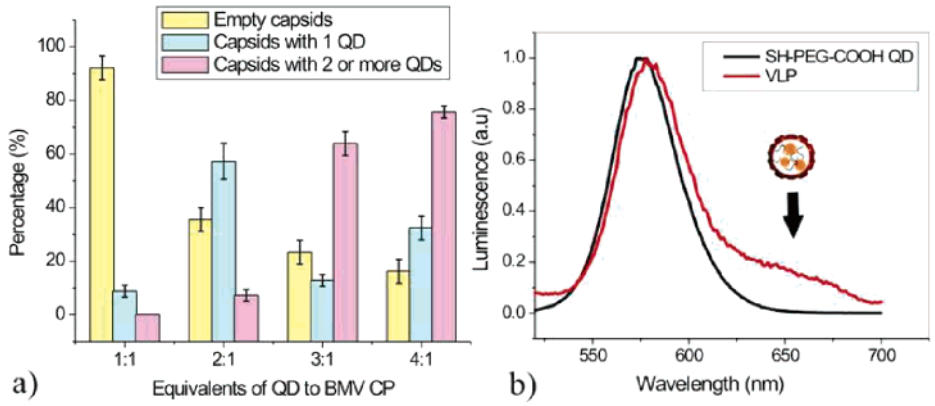

Figure 7. (a) Comparison of assembly of BMV with 1, 2, 3, and 4 equivalents of HS-PEG-COOH-coated QDs. (b) Fluorescence spectra of VLP with HS-PEG-COOH-coated QDs versus HS-PEG-COOH coated QDs. The shoulder observed between 625 and 700 nm is likely due to the coupling of multiple encapsulated QDs.[38]

At 4 equivalents of PEG-coated cores, the assembly reaction contained more incompletely formed capsids and some protein/QD amorphous aggregation (data not shown). A similar phenomenon has been observed in the formation of VLP with Au cores; when the cores are presenting excess, incomplete protein coverage occurs.[10] Incomplete QD/protein complexes are likely to have sticky, hydrophobic surfaces that would account for the observed propensity to aggregate.

Fluorescence measurements of VLPs with HS-PEG-COOH-coated QDs (Figure 7b) showed an emission wavelength shift of around 3−5 nm with respect to HS-PEG-COOH-coated QDs alone. We hypothesize that the encapsidation of HS-PEG-COOH-coated QDs in the viral capsid causes an increase in the effective index of refraction ($n \sim 1.5$).[39] Also, there is a new broad feature in the emission spectra of VLP with HS-PEG-COOH-coated QDs, which might be due to coupling between two or more QDs packaged within a VLP.[38]

Conclusion. Four types of molecular coatings of QDs have been studied with respect to their photostability at prolonged ultraviolet light exposures and their incorporation in BMV capsids. HS-PEG-COOH coatings were the most photostable to prolonged short-wavelength visible radiation in comparison to coatings consisting of phospholipids, DNA, or DHLA. The HS-PEG-COOH coating also shows the highest ability in promoting virus capsid assembly. Multiple functionalized QDs can be encapsulated by self-assembly in viral capsids, yielding a virus-like particle similar in size with the native virus. Encapsulation of several functionalized QDs inside each VLP is due to the smaller size of QDs compared to similarly functionalized gold nanoparticles reported earlier. These results support a thesis that rules for encapsidation learned from gold nanoparticles can be directly applied to the encapsidation of other cores with desired properties. Furthermore, manipulations of the diameter of the packaged material can be used to achieve the degree of packaging. Last, because PEG properties are easier to control than other coatings, especially coatings consisting of biological macromolecules, the use of PEG-coated cores should facilitate additional industrial processes that require nanoparticles of uniform sizes and yet have a protein coat that can be manipulated for the desired specificity by molecular engineering.

Acknowledgment. We gratefully acknowledge support from NSF grant BES 0322767 (B.D.) and NIH grant GM59249 (VR).

References

(1) Michalet, X.; Pinaud, F. F.; Bentolila, L. A.; Tsay, J. M.; Doose, S.; Li, J. J.; Sundaresan, G.; Wu, A. M.; Gambhir, S. S.; Weiss, S. *Science* **2005**, *307*, 538−544.
(2) Sukhanova, A.; Devy, J.; Venteo, L.; Kaplan, H.; Artemyev, M.; Oleinikov, V.; Klinov, D.; Pluot, M.; Cohen, J. H. M.; Nabiev, I. *Anal. Biochem.* **2004**, *324*, 60−67.
(3) Zanchet, D.; Micheel, C. M.; Parak, W. J.; Gerion, D.; Alivisatos, A. P. *Nano Lett.* **2001**, *1*, 32−35.
(4) Gao, X. H.; Chan, W. C. W.; Nie, S. M. *J. Biomed. Opt.* **2002**, *7*, 532−537.
(5) Seisenberger, G.; Ried, M. U.; Endre, T.; Buning, H.; Hallek, M.; Brauchle, C. *Science* **2001**, *294*, 1929−1932.
(6) Lakadamyali, M.; Rust, M.; Babcock, H.; Zhang, F.; Zhuang, X. W. *Biophys. J.* **2003**, *84*, 583A−583A.
(7) Agrawal, A.; Zhang, C.; Byassee, T.; Tripp, R. A.; Nie, S. *Anal. Chem.* **2006**, *78*, 1061−1070.
(8) Agrawal, A.; Tripp, R. A.; Anderson, L. J.; Nie, S. M. *J. Virol.* **2005**, *79*, 8625−8628.
(9) Dragnea, B.; Chen, C.; Kwak, E. S.; Stein, B.; Kao, C. C. *J. Am. Chem. Soc.* **2003**, *125*, 6374−6375.
(10) Chen, C.; Kwak, E. S.; Stein, B.; Kao, C. C.; Dragnea, B. *J. Nanosci. Nanotechnol.* **2005**, *5*, 2029−2033.
(11) Chen, C.; Daniel, M.-C.; Quinkert, Z.; De, M.; Stein, B.; Chipman, P. R.; Rotello, V. M.; Kao, C. C.; Dragnea, B. *Nano Lett.* **2006**, *6*, 611−616.
(12) Loo, L.; Guenther, R. H.; Basnayake, V. R.; Lommel, S. A.; Franzen, S. *J. Am. Chem. Soc.* **2006**, *128*, 4502−4503.
(13) Lucas, R. W.; Larson, S. B.; McPherson, A. *J. Mol. Biol.* **2002**, *317*, 95−108.
(14) Alexander, M. *BioEssays* **2005**, *27*, 447−458.
(15) Derfus, A. M.; Chan, W. C. W.; Bhatia, S. N. *Nano Lett.* **2004**, *4*, 11−18.
(16) P. Pfeiffer; M. Herzog; Hirth, L. *Philos. Trans. R. Soc.* **1976**, *276*, 99−107.
(17) Hines, M. A.; Guyot-Sionnest, P. *J. Phys. Chem.* **1996**, *100*, 468−471.
(18) Dubertret, B.; Skourides, P.; Norris, D. J.; Noireaux, V.; Brivanlou, A. H.; Libchaber, A. *Science* **2002**, *298*, 1759−1762.
(19) Fu, A. H.; Micheel, C. M.; Cha, J.; Chang, H.; Yang, H.; Alivisatos, A. P. *J. Am. Chem. Soc.* **2004**, *126*, 10832−10833.
(20) Damayanti, T. A.; Tsukaguchi, S.; Mise, K.; Okuno, T. *J. Virol.* **2003**, *77*, 9979−9986.
(21) Goldman, E. R.; Balighian, E. D.; Mattoussi, H.; Kuno, M. K.; Mauro, J. M.; Tran, P. T.; Anderson, G. P. *J. Am. Chem. Soc.* **2002**, *124*, 6378−6382.

(22) Hong, R.; Fischer, N. O.; Verma, A.; Goodman, C. M.; Emrick, T.; Rotello, V. M. *J. Am. Chem. Soc.* **2004**, *126*, 739−743.
(23) Rao, A. L. N.; Dugall, R.; Lahser, F. C.; Hall, T. C. *Methods Mol. Genet.* **1994**, *4*, 216−236.
(24) Ludtke, S. J.; Baldwin, P. R.; Chiu, W. *J. Struct. Biol.* **1999**, *128*, 82−97.
(25) Pettersen, E. F.; Goddard, T. D.; Huang, C. C.; Couch, G. S.; Greenblatt, D. M.; Meng, E. C.; Ferrin, T. E. *J. Comput. Chem.* **2004**, *25*, 1605−1612.
(26) Johnsson, M.; Hansson, P.; Edwards, K. *J. Phys. Chem. B* **2001**, *105*, 8420−8430.
(27) Fernández-Nieves, A.; Fernández-Barbero, A.; de las Nieves, F. J. *Phys. Rev. E* **2001**, *63*, 041404.
(28) Manna, L.; Scher, E. C.; Li, L. S.; Alivisatos, A. P. *J. Am. Chem. Soc.* **2002**, *124*, 7136−7145.
(29) Cordero, S. R.; Carson, P. J.; Estabrook, R. A.; Strouse, G. F.; Buratto, S. K. *J. Phys. Chem. B* **2000**, *104* , 12137−12142.
(30) Myung, N.; Bae, Y.; Bard, A. J. *Nano Lett.* **2003**, *3*, 747−749.
(31) Hiebert, E.; Bancroft, J. B.; Bracker, C. E. *Virology* **1968**, *34*, 492−508.
(32) Butler, P. J. G. *Nature* **1975**, *255*.
(33) Choi, Y. G.; Rao, A. L. N. *Virology* **2000**, *275*, 249−257.
(34) Choi, Y. G.; Rao, A. L. N. *Virology* **2000**, *275*, 207−217.
(35) Annamalai, P.; Rao, A. L. N. *Virology* **2005**, *338*, 96−111.
(36) Onafuwa-Nuga, A. A.; Telesnitsky, A.; King, S. R. *RNA* **2006**, *12*, 542−546.
(37) Krol, M. A.; Olson, N. H.; Tate, J.; Johnson, J. E.; Baker, T. S.; Ahlquist, P. *Proc. Natl. Acad. Sci. U.S.A.* **1999**, *96*, 13650−13655.
(38) Mikhailovsky, A. A.; Malko, A. V.; Hollingsworth, J. A.; Bawendi, M. G.; Klimov, V. I. *Appl. Phys. Lett.* **2002**, *80*, 2380−2382.
(39) Terrettaz, S.; Ulrich, W.-P.; Vogel, H.; Hong, Q.; Dover, L. G.; Lakey, J. H. *Protein Sci* **2002**, *11*, 1917−1925.

NL061165U